

The environs of the ultracompact HII region G45.45+0.06

S. Paron¹, S. Cichowolski¹, and M. E. Ortega¹

Instituto de Astronomía y Física del Espacio (IAFE), CC 67, Suc. 28, 1428 Buenos Aires, Argentina
e-mail: sparon@iafe.uba.ar

Received ;date; Accepted ;date;

ABSTRACT

Aims. G45.45+0.06 is an ultra-compact HII (UCHII) region extensively studied. It is known that G45.45+0.06 is embedded in a complex of UCHII regions, but up to the date, the surrounding ISM in a larger spatial scale has not been analyzed.

Methods. Using data from large-scale surveys: Two Micron All Sky Survey, GLIMPSE, MIPS GAL, MAGPIS and GRS, we performed a multiwavelength study of a region about $7' \times 7'$ in the vicinity of G45.45+0.06.

Results. We found that the UCHII complex lies in a border of a larger (diameter of $\sim 3'$) and fainter HII region, which is located at the same distance as G45.45+0.06, ~ 8 kpc. In this work, this larger HII region was called G45L. A good morphological correlation is observed between the PDRs and the molecular gas mapped in the ^{13}CO J=1–0 and CS J=2–1 lines, suggesting that G45L may be collecting the molecular material. From a near- and mid-IR photometric study, we found three sources, likely O-type stars, that are possibly responsible for the creation of G45L. Additionally we found several YSO candidates lying preferentially in the molecular shell that surrounds G45L. Our results confirm that the region southeastern the UCHII complex where G45.45+0.06 is embedded and eastern G45L is active in star formation. We suggest that G45L has been expanding during about 2×10^6 yr and could have triggered the formation of the zero-age main sequence stars that are ionizing the UCHII region G45.45+0.06. However we can not discard that both HII regions are coeval.

Key words. ISM: HII regions – ISM: clouds – stars: formation

1. Introduction

Nowadays it is well established that the formation of massive stars can be triggered by the action of expanding HII regions through the “collect and collapse” process. During its supersonic expansion, an HII region can collect a dense layer of material between its ionization and shock fronts. This layer can be fragmented in massive condensations that

then may collapse to lead to the formation of new stars. Thus, it is expectable the presence of protostars, young stars, and ultra-compact HII (UCHII) regions on the borders of HII regions. Several observational evidence have been found supporting this star forming mechanism (see e.g. Pomarès et al. 2009; Zavagno et al. 2007, and reference therein).

G45.45+0.06 is a luminous Galactic UCHII region that has been extensively studied in the radio continuum and in molecular lines (e.g. Wood et al. 1988; Garay et al. 1993; Wilner et al. 1996; Hatchell et al. 1998). This UCHII region presents CH₃OH and H₂O maser emission (Codella et al. 2004). Recently, G45.45+0.06 was included in the Boston University Catalog of Galactic HII Region Properties (Anderson et al. 2009). Using the ¹³CO J=1–0 emission obtained from the GRS¹, the authors derive a $v_{\text{LSR}} \sim 55.6 \text{ km s}^{-1}$ and a kinematical distance of 8.2 kpc for this UCHII region, in agreement, within errors, with previous estimations (e.g. $v_{\text{LSR}} \sim 55.9 \text{ km s}^{-1}$ and $d \sim 7.7 \text{ kpc}$, Kolpak et al. 2003). As early proposed by Matthews et al. (1977), G45.45+0.06 is part of a cluster of several UCHII regions. Giveon et al. (2005a,b) generated a catalog matching VLA Galactic plane catalogs at 5 and 1.4 GHz with new radio continuum observations and the MSX6C Galactic plane catalog. According to this catalog, G45.45+0.06 is part of a complex of five radio compact HII regions. Feldt et al. (1998) performed a near- and mid-infrared study of G45.45+0.06 and concluded that this UCHII region, the oldest in the complex, is a young OB cluster around which sequential star formation is taking place. Recently, Blum & McGregor (2008) using NIFS behind ALTAIR on Gemini North identified several massive O-type stars that are ionizing G45.45+0.06. The complexity of this region is evident. Moreover, in the vicinity of this complex (see Figure 1), Cyganowski et al. (2008) discovered an “extended green object” (EGO), a source with extended *Spitzer*-IRAC 4.5 μm emission which is usually presented in green colour. According to the authors, an EGO is a massive young stellar object (MYSO) driven outflows. The presence of this EGO reveals that star formation is taking place in this region. Indeed, this EGO coincides with the high-mass star forming region G45.47+0.05 studied by Remijan et al. (2004).

In this work, we present a multiwavelength study of the spatial environment surrounding the UCHII region G45.45+0.06, with the purpose of exploring the ISM around the complex. We use survey and archival data to show that G45.45+0.06 is located in the environs of a larger HII region whose expansion could have originated the conditions for the formation of the UCHII region G45.45+0.06.

2. Data

The data presented and analyzed in this work were extracted from five large-scale surveys: Two Micron All Sky Survey (2MASS)², Galactic Legacy Infrared Mid-Plane Survey Extraordinaire (GLIMPSE), MIPS GAL, MAGPIS and GRS. GLIMPSE is a mid infrared survey of the inner Galaxy performed using the *Spitzer Space Telescope*. We used the mo-

¹ Galactic Ring Survey (Jackson et al. 2006)

² 2MASS is a joint project of the University of Massachusetts and the Infrared Processing and Analysis Center/California Institute of Technology, funded by the National Aeronautics and Space Administration and the National Science Foundation.

saiced images from GLIMPSE and the GLIMPSE Point-Source Catalog (GPSC) in the *Spitzer*-IRAC (3.6, 4.5, 5.8 and 8 μm). IRAC has an angular resolution between $1''.5$ and $1''.9$ (see Fazio et al. 2004 and Werner et al. 2004). MIPS GAL is a survey of the same region as GLIMPSE, using MIPS instrument (24 and 70 μm) on *Spitzer*. The MIPS GAL resolution at 24 μm is $6''$. MAGPIS is a radio continuum survey of the Galactic plane at 6 and 20 cm using the VLA in configurations B, C and D combined with the Effelsberg 100 m single-dish telescope (White et al. 2005). The GRS is being performed by the Boston University and the Five College Radio Astronomy Observatory (FCRAO). The survey maps the Galactic Ring in the ^{13}CO J=1–0 line with an angular and spectral resolution of $46''$ and 0.2 km s^{-1} , respectively (see Jackson et al. 2006). The observations were performed in both position-switching and On-The-Fly mapping modes, achieving an angular sampling of $22''$. We also analyzed the additional data that this survey presents: the CS J=2–1 line, which has similar angular and spectral resolutions as the ^{13}CO J=1–0 line.

3. Results and discussion

Figure 1 shows a *Spitzer*-IRAC three color image as extracted from GLIMPSE of a region about $7' \times 7'$ in the vicinity of the UCHII complex where G45.45+0.06 lies. The three IR bands are 3.6 μm (in blue), 4.5 μm (in green) and 8 μm (in red). The contours correspond to the ^{13}CO J=1–0 emission as extracted from the GRS integrated between 50 and 65 km s^{-1} , a velocity range around the v_{LSR} of G45.45+0.06. The UCHII complex lies on a border of a more extended structure as seen mainly in the *Spitzer*-IRAC 8 μm band. The morphological correlation between the 8 μm , mainly originated in the polycyclic aromatic hydrocarbons (PAHs), and the molecular gas is suggestive of an expansive and “collective” HII region. It is important to note that the PAHs emission delineates the HII region boundaries. This is because these molecules are destroyed inside the ionized region, but are excited in the photodissociation region (PDR) by the radiation leaking from the HII region (Pomarès et al. 2009).

Although G45L is not completely bordered by a PDR, its morphology resembles the structure of the IR dust bubbles associated with O and early-B type stars: a PDR visible in the 8 μm band, which encloses ionized gas observed at 20 cm and hot dust observed at 24 μm (see Churchwell et al. 2006, 2007; Watson et al. 2008). Figure 2 (left) displays a composite two color image, where the red represents the *Spitzer*-IRAC 8 μm band and the green the above 3σ radio continuum emission at 20 cm extracted from MAGPIS. The high angular resolution of the MAGPIS 20 cm image allows us to distinguish two different radio continuum structures: that associated with the UCHII complex, where both colors are combined and saturated (yellow), and other more diffuse towards the West, enclosed by the 8 μm emission that indicates the photodissociation regions (PDRs). Hereafter, this latter structure, an HII region of about $3'$ in diameter, possible related to the molecular gas shown in Figure 1 as contours, will be called G45L. As indicated in Figure 2 (left), the brightest part of the radio continuum diffuse structure located at $l \sim 45^\circ.42, b \sim 0^\circ.072$ is bordered by two PDRs: the North and the middle PDRs. Towards the South, the HII region is fainter and bordered by what we called South PDR. Figure 2 (right) shows a two

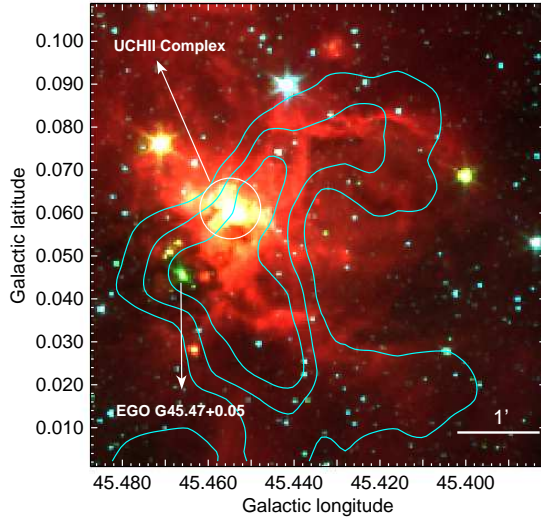


Fig. 1. *Spitzer*-IRAC three color image ($3.5 \mu\text{m}$ = blue, $4.5 \mu\text{m}$ = green and $8 \mu\text{m}$ = red). The contours correspond to the ^{13}CO J=1–0 emission as extracted from the GRS integrated between 50 and 65 km s^{-1} , the levels are 27, 37 and 48 K km s^{-1} . The UCHII complex is remarked with a circle. Also, the EGO discovered by Cyganowski et al. (2008) is indicated. The angular resolutions are $\sim 1''.5$ and $\sim 46''$ for the *Spitzer* and molecular data, respectively.

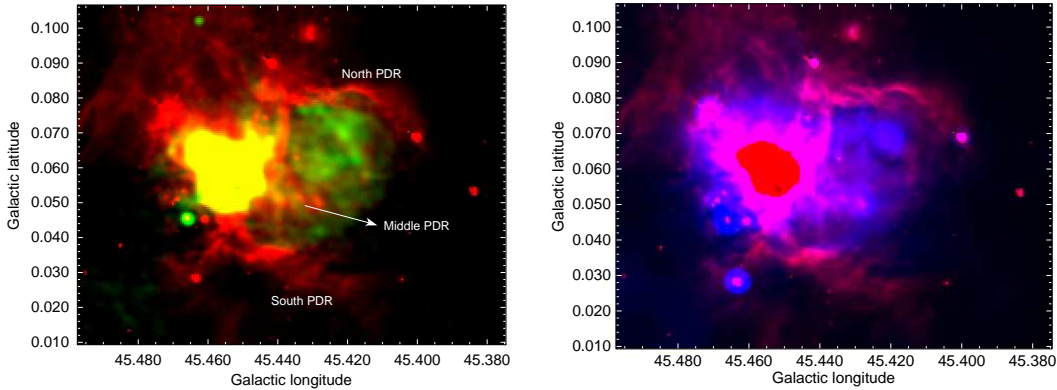


Fig. 2. Two color images. Left: the red is the *Spitzer*-IRAC $8 \mu\text{m}$ emission and the green is the above 3σ radio continuum emission at 20 cm extracted from MAGPIS. Yellow is the superposition of the IR and radio continuum emissions. Right: the red is the same as the left image and the blue represents the MIPSGAL emission at $24 \mu\text{m}$. The red structure onto the UCHII complex is not real, it is just due to the presence of saturated pixels of the MIPSGAL emission.

color image where again the red is the *Spitzer*-IRAC $8 \mu\text{m}$ emission and the blue represents the MIPSGAL emission at $24 \mu\text{m}$. The red structure observed onto the UCHII complex is not real, it is just due to the presence of saturated pixels in the MIPSGAL image.

3.1. Distance

We are studying a region in the first Galactic quadrant, thus we have to take into account the distance ambiguity that exists when using radial velocities and a Galactic rotation curve to assign distances to sources. According to Kolpak et al. (2003) and Anderson et al. (2009), G45.45+0.06 has a radio recombination line velocity of $\sim 56 \text{ km s}^{-1}$, which gives the

possible distances of ~ 4 or ~ 8 kpc. As the HI absorption spectrum towards G45.45+0.06 presents an absorption feature at the tangent point velocity (~ 64 km s $^{-1}$), the authors adopted the farther distance for G45.45+0.06.

The molecular gas belonging to the shell associated with G45L (see Figure 1) is at the same velocity range as the gas related to the UCHII complex where G45.45+0.06 is embedded, which may suggest that G45L is at the same distance as the UCHII complex. In order to prove this suggestion, using HI data extracted from the VLA Galactic Plane Survey (VGPS) (Stil et al. 2006), we studied the absorption features towards two regions: the UCHII complex where G45.45+0.06 is embedded (Figure 3-up) and the radio continuum structure enclosed by North and middle PDR (Figure 3-down). As both profiles have the same HI absorption features, we conclude that G45L is at the same distance as G45.45+0.06. Hereafter we adopt the distance of 8 kpc.

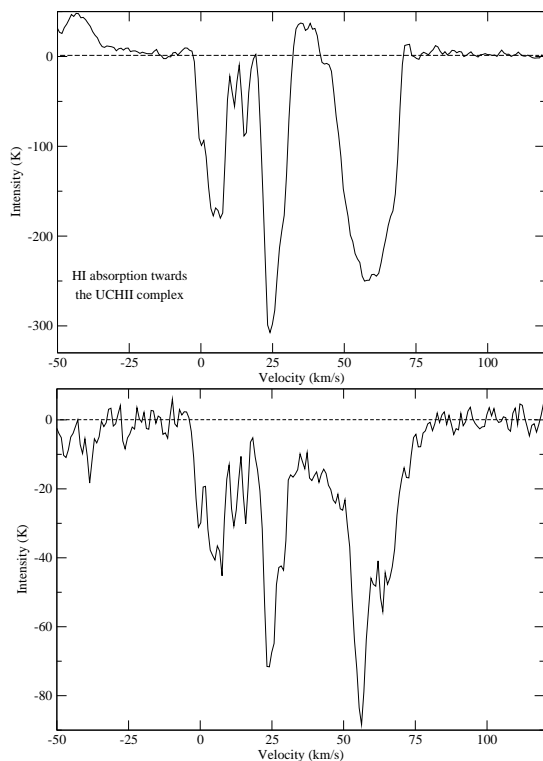


Fig. 3. Up: HI absorption towards the UCHII complex where G45.45+0.06 is embedded. Down: HI absorption towards the radio continuum structure enclosed by North and middle PDR. Note that both profiles have the same HI absorption features.

3.2. Molecular Environment

As shown in Figure 1, an incomplete ^{13}CO shell at the velocity range between 50 and 65 km s $^{-1}$ presents a good morphological correlation with the North and South PDRs visible in the 8 μm band (see Figure 2-left). This suggests that the expansion of the HII region, that we called G45L, is collecting the molecular gas as is observed in other HII regions (e.g. Pomarès et al. 2009; Cichowolski et al. 2009; Deharveng et al. 2008). Figure 4 shows the integrated velocity channel maps of the ^{13}CO J=1–0 emission every ~ 1.25 km s $^{-1}$. For

reference, the circle highlights the position and the size of G45L as suggested by the North and South PDRs. From this figure is clear that the molecular gas is more abundant towards the East. In particular, the $v = 58.1 \text{ km s}^{-1}$ channel map shows two molecular clumps spatially coincident with the UCHII complex and the region where the EGO G45.47+0.05 lies, respectively. It is also evident that the molecular gas encompasses the circle, showing the velocity structure of the molecular shell related to G45L. As Deharveng et al. (2005) propose, the presence of a molecular shell surrounding the ionized gas of an HII region, or the presence of massive fragments regularly spaced along the ionization front, suggest that the collect and collapse process is at work in the region. On the other hand, the channels with velocities of 56.8 and 58.1 km s^{-1} show a smaller molecular shell interior to the circle and in spatial coincidence with the structure delimited by the middle and North PDRs (see Figure 2-left).

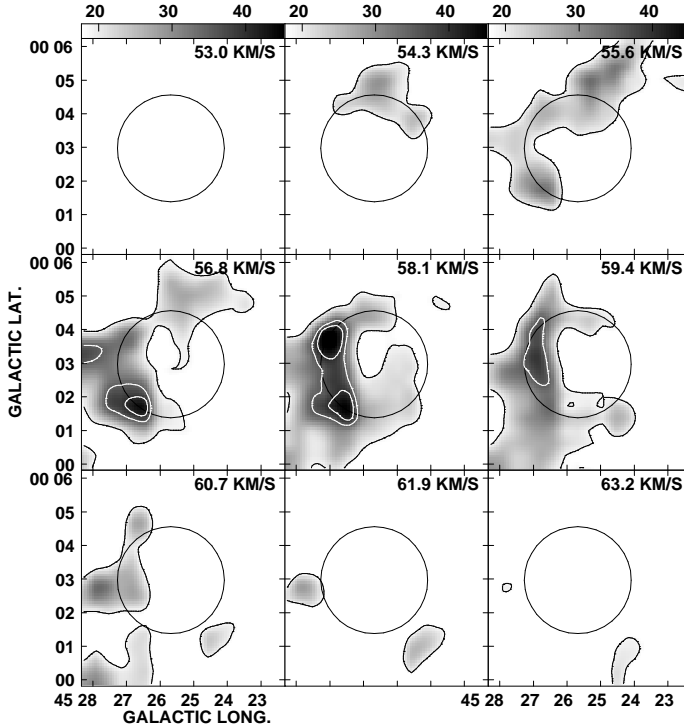


Fig. 4. Integrated velocity channel maps of the ^{13}CO $J=1-0$ emission every $\sim 1.25 \text{ km s}^{-1}$. The grayscale is displayed at the top of the figure and is in K km s^{-1} , the contour levels are 5, 9.5 and 11 K km s^{-1} . Note that the molecular gas encompasses the circle, which highlights the position and size of G45L as suggested by the North and South PDRs (see Figure 2-left).

Figure 5 displays the CS $J=2-1$ emission integrated between 54 and 66 km s^{-1} . The CS $J=2-1$ emission presents a similar structure as the ^{13}CO . Given that this line requires high densities, $10^4 - 10^5 \text{ cm}^{-3}$, to be excited (see e.g. Luna et al. 2006), its detection indicates the presence of high density gas in the molecular shell, mainly towards the East.

In order to analyze the kinematics of the molecular gas, we study the molecular spectra from three different regions: Region 1 (the North portion of the molecular shell, in coincidence with the North PDR), Region 2 (the South portion of the molecular shell,

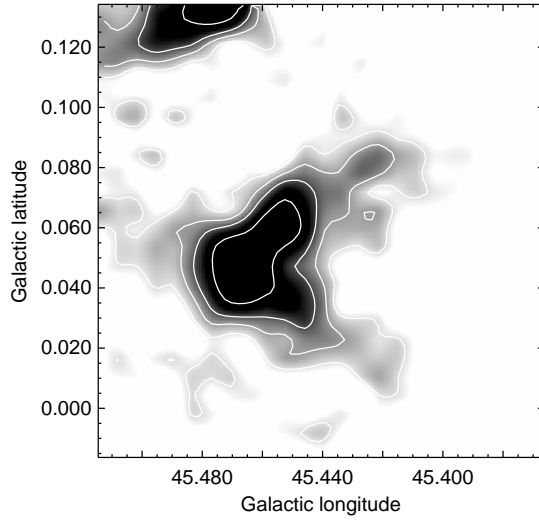


Fig. 5. CS J=2–1 emission integrated between 54 and 66 km s⁻¹. The contour levels are 2.4, 3.6, 5 and 8 K km s⁻¹. Note that the CS emission presents a similar structure as the ¹³CO.

in coincidence with the South PDR) and Region 3 (where the molecular emission peaks). Figure 6 (left) shows the *Spitzer*-IRAC 8 μ m emission with contours of the integrated ¹³CO J=1–0 as presented in Figure 1. Regions 1, 2 and 3 are indicated with boxes of approximately 2' \times 1/8', 2/2 \times 1/2' and 1/5 \times 2/5' in size, respectively. Towards the right, the ¹³CO J=1–0 and CS J=2–1 average spectra corresponding to the emission of each region are displayed. Between 40 and 50 spectra were averaged to obtain each average emission spectrum. The parameters determined from Gaussian fitting of these lines are presented in Table 1. T_{mb} represents the peak brightness temperature, V_{lsr} the central velocity, Δv the line width and I the integrated line intensity. Errors are formal 1 σ value for the model of the Gaussian line shape. The ¹³CO and CS average lines corresponding to Region 1 were best fitted with two Gaussians.

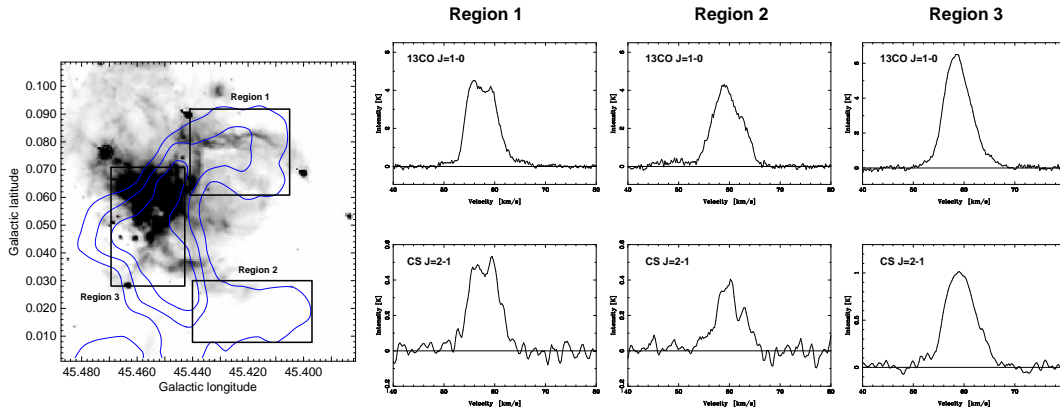
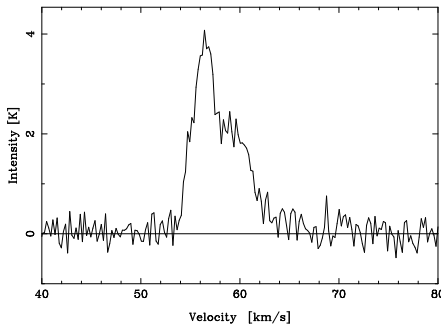


Fig. 6. Left: *Spitzer*-IRAC 8 μ m emission with contours of the integrated ¹³CO J=1–0 as presented in Figure 1. The boxes represent the regions from which were obtained the average of the molecular emissions. Towards the right the ¹³CO J=1–0 and CS J=2–1 average spectra from each region are shown. The rms noise are \sim 0.03 and \sim 0.04 K for the ¹³CO and CS, respectively.

Table 1. Observed parameters of the ^{13}CO J=1–0 and CS J=2–1 average emissions towards the regions shown in Figure 6.

Emission	T_{mb} (K)	V_{lsr} (km s^{-1})	Δv (km s^{-1})	I (K km s^{-1})
<i>Region 1</i>				
^{13}CO J=1–0	3.80 ± 0.50	58.75 ± 1.05	5.05 ± 0.25	17.00 ± 3.00
	4.10 ± 0.50	55.25 ± 1.05	3.00 ± 0.15	15.00 ± 2.00
CS J=2–1	0.46 ± 0.11	59.60 ± 1.10	4.00 ± 0.20	2.00 ± 0.30
	0.42 ± 0.15	55.80 ± 1.10	3.45 ± 0.15	1.90 ± 0.30
<i>Region 2</i>				
^{13}CO J=1–0	4.10 ± 0.50	59.50 ± 0.50	6.75 ± 0.85	30.00 ± 3.80
CS J=2–1	0.35 ± 0.05	59.90 ± 0.50	6.25 ± 0.95	2.30 ± 0.50
<i>Region 3</i>				
^{13}CO J=1–0	6.40 ± 0.50	58.65 ± 0.25	6.10 ± 0.50	41.50 ± 3.50
CS J=2–1	1.00 ± 0.10	59.25 ± 0.55	7.00 ± 1.00	7.70 ± 1.50

Besides, taking into account that the ^{13}CO J=1–0 beam ($46''$) covers completely the middle PDR, we present in Figure 7 a spectrum obtained from $l = 45^\circ 430, b = 0^\circ 055$. This spectrum shows the molecular emission probably related to the middle PDR. The velocity of the main component of this profile is $v \sim 56 \text{ km s}^{-1}$, in coincidence with one of the two molecular components of the North PDR (Region 1 in Figure 6). The spectrum is not symmetrical: it presents another weaker component or a wing towards larger velocities.

**Fig. 7.** ^{13}CO J=1–0 spectrum obtained towards the middle PDR, at $l = 45^\circ 430, b = 0^\circ 055$. The main component velocity is $v \sim 56 \text{ km s}^{-1}$, which coincides with one of the two molecular components of the North PDR.

The molecular spectra analysis shows that the North PDR has associated two possible molecular structures centered at $v \sim 55 \text{ km s}^{-1}$ and $v \sim 59 \text{ km s}^{-1}$, respectively. The main velocity component of the molecular gas associated with the middle PDR is centered at $v \sim 55 \text{ km s}^{-1}$, while the molecular gas related to the South PDR is centered at $v \sim 59 \text{ km s}^{-1}$. If the molecular gas is indeed associated with G45L, this may suggest that we have to take into account projection effects to understand the three dimensional structure of G45L. This will be discussed in Section 3.5.

Using the ^{13}CO J=1–0 line and assuming local thermodynamic equilibrium (LTE) we estimate the H_2 column density towards the three regions shown in Figure 6. We use:

$$N(^{13}\text{CO}) = 2.42 \times 10^{14} \frac{T_{\text{ex}} \int \tau_{13} dv}{1 - \exp(-5.29/T_{\text{ex}})}$$

to obtain the ^{13}CO column density. τ_{13} is the optical depth of the line and following Anderson et al. (2009) the T_{ex} was assumed to be 13 K. We assume the ^{13}CO emission is optically thin and use the Gaussian fit line parameters (Table 1) to find the optical depth integral. Finally, we use the relation $N(\text{H}_2)/N(^{13}\text{CO}) \sim 5 \times 10^5$ (e.g. Simon et al. 2001) to estimate the following values: $N(\text{H}_2) \sim 1.5 \times 10^{22} \text{ cm}^{-2}$ for Region 1 and 2, respectively and $N(\text{H}_2) \sim 2.8 \times 10^{22} \text{ cm}^{-2}$ for Region 3.

In addition we estimate the CS column densities, $N(\text{CS})$, towards these regions. Although the CS J=2–1 line is generally optically thick, a lower limit to the $N(\text{CS})$ can be estimated under the assumption of optically thin CS emission. We use the following equation (Ohashi et al. 1991):

$$N(\text{CS}) = 8.5 \times 10^{11} \frac{\exp(2.4/T_{\text{ex}})}{1 - \exp(-4.7/T_{\text{ex}})} \times T_{\text{mb}} \times \Delta v,$$

where T_{mb} is the CS brightness temperature and Δv is the velocity width of the CS line. Following Goicoechea et al. (2006), who studied the Horsehead PDR using CS J=2–1 between other molecular lines, we assume $T_{\text{ex}} = 9$ K. We obtain $N(\text{CS}) \sim (8 \text{ and } 6) \times 10^{12} \text{ cm}^{-2}$ for Region 1 and 2, respectively, and $N(\text{CS}) \sim 2 \times 10^{13} \text{ cm}^{-2}$ for Region 3.

From the H_2 and CS column densities, we can estimate the CS abundances, $X(\text{CS}) = N(\text{CS})/N(\text{H}_2)$. We obtain $X(\text{CS}) \sim (5, 3.5 \text{ and } 7) \times 10^{-10}$ for Region 1, 2 and 3, respectively. Taking into account the LTE approximation and that the estimated CS column densities are lower limits, these values are comparable with those obtained towards the Orion Bar (a warm PDR), $X(\text{CS}) \sim 2.9 \times 10^{-9}$ (Johnstone et al. 2003) and towards the Horsehead PDR, $X(\text{CS}) \sim (7 \pm 3) \times 10^{-9}$ (Goicoechea et al. 2006). New CS and C^{34}S observations in several lines would be very useful to study the sulfur depletion in G45L PDRs.

Finally, we estimate the total mass of the whole molecular shell in $M \sim 10^5 M_{\odot}$. This value was obtained from:

$$M = \mu m_{\text{H}} \sum [D^2 \Omega N(\text{H}_2)],$$

where Ω is the solid angle subtended by the ^{13}CO J=1–0 beam size, m_{H} is the hydrogen mass, μ , the mean molecular weight, is assumed to be 2.8 by taking into account a relative helium abundance of 25 %, and D is the distance. Summation was performed over all the observed positions within the 27 K km s^{-1} contour level (see Figures 1 and 6).

3.3. The exciting star(s) of G45L

Given that we do not find any cataloged massive star in the area that may be related to G45L, we have used the GLIMPSE I Spring'07 Catalog to analyze the infrared sources seen in projection onto G45L to identify the star(s) responsible for its creation. Considering only the sources that have been detected in the four Spitzer-IRAC bands, we found 14 sources towards the region located inside the observed PDRs. The main parameters of these sources are shown in Table 2. Figure 8 indicates the location of the sources with respect

to the emission distribution at $8 \mu\text{m}$ (red) and the radio continuum at 20 cm (green). To examine the evolutionary stage of these sources, we analyze their location onto a color-color IRAC diagram as shown in Figure 9. Following Allen et al. (2004) color criteria, we found that 8 sources could be classified as main sequence stars (Class III). Among these sources we look for O-type stars as responsible for ionizing the surrounding gas. Using the J , H and K apparent magnitudes as obtained from the 2MASS Point Source Catalog, we estimate the absolute magnitudes for the mentioned 8 sources. To convert the apparent magnitudes in absolute ones, we assume a distance of 8 kpc and a visual absorption between 8 and 12 mag. The extinction values were obtained by inspecting the infrared sources location onto the color-color diagram ($H-K$) vs ($J-H$) (not presented here). By comparing the estimated absolute magnitudes with those tabulated by Martins & Plez (2006), we found that sources #1, #9 and #14 are probably O-type stars (likely between O4V and O8V), which is consistent with their position in the color-magnitude diagram K vs ($H-K$) (not presented here). Source #1 is slightly displaced towards the region of giants stars in the color-magnitude diagram, but it could be a reddened O-type star. An inspection of Figure 8 shows that sources #1 and #9 are located almost onto the central part of G45L, while source #14 lies towards its boundary. This fact suggest that sources #1 and #9 are the most promising candidates for being related to G45L. In particular, source #9 is projected onto a local minimum observed in the brightest part of the G45L radio continuum emission, suggesting that this source could have been blowing its environs creating a small cavity around it.

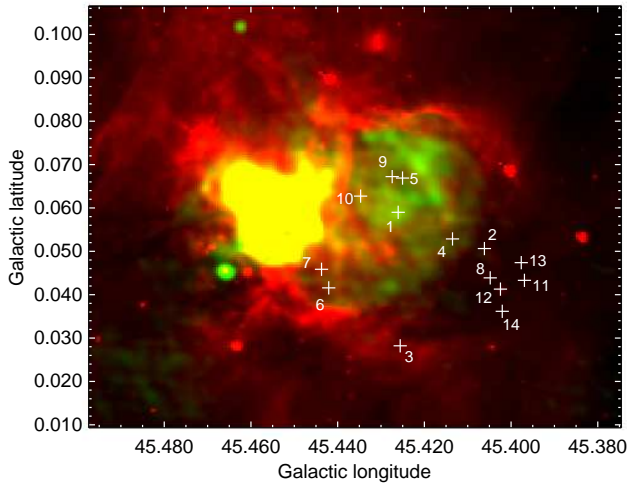


Fig. 8. Colour composite image, with the radio continuum emission at 1420 MHz in green, and the infrared emission at $8 \mu\text{m}$ in red. Yellow is the superposition of the IR and radio continuum emissions. The exciting stars candidates are identified (see Table 2).

In order to investigate if these three sources can provide the energy necessary to ionize the gas, we need to estimate the radio continuum flux of G45L. Using the radio continuum emission data at 1420 MHz, we estimate a flux density of $S_{1420\text{MHz}} \sim 1.0 \pm 0.2$ Jy for G45L. The number of UV photons necessary to keep the gas ionized is derived using $N_{UV}(\text{photons s}^{-1}) = 0.76 \times 10^{47} T_4^{-0.45} \nu_{\text{GHz}}^{0.1} S_\nu D_{\text{kpc}}^2$ (Chaisson 1976), where T_4 is the elec-

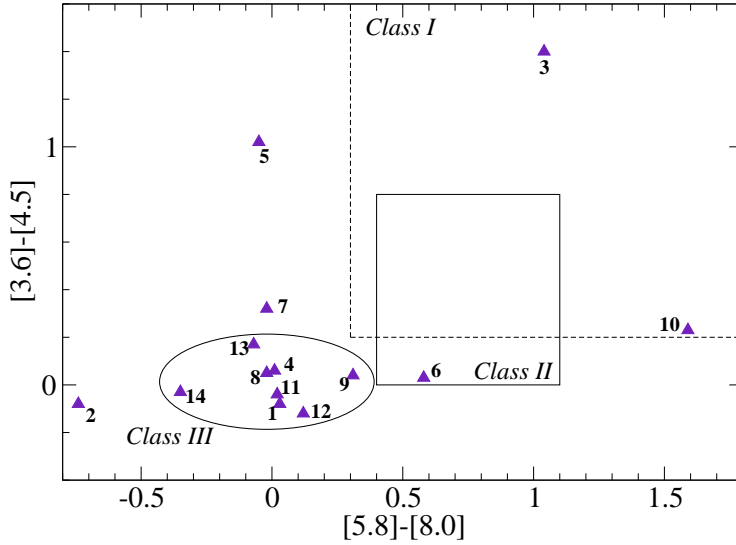


Fig. 9. GLIMPSE-IRAC color-color diagram $[3.6] - [4.5]$ versus $[5.8] - [8.0]$ for the sources displayed in Figure 8. Class I, II and III regions are indicated following Allen et al. (2004). The ellipse (Class III region: main sequence and giant stars) encloses the sources that we consider to be possible exciting star(s) of G45L.

Table 2. Main parameters of the infrared sources found towards G45L.

#	Glimpse designation	Galactic coordinates	J	H	K_S	$3.6 \mu\text{m}$	$4.5 \mu\text{m}$	$5.8 \mu\text{m}$	$8.0 \mu\text{m}$	Notes
1	G045.4260+00.0590	$45^\circ 426, 0^\circ 058$	13.93	11.89	11.08	10.47	10.55	10.21	10.18	Class III - (O-type)
2	G045.4061+00.0506	$45^\circ 406, 0^\circ 050$	13.13	11.67	11.08	10.71	10.79	10.58	11.32	
3	G045.4255+00.0282	$45^\circ 425, 0^\circ 028$	null	null	null	13.7	12.3	11.09	10.05	
4	G045.4135+00.0528	$45^\circ 413, 0^\circ 052$	11.51	10.45	10.09	9.86	9.8	9.69	9.68	Class III
5	G045.4250+00.0668	$45^\circ 425, 0^\circ 066$	null	null	14.43	11.33	10.31	9.77	9.81	
6	G045.4420+00.0415	$45^\circ 442, 0^\circ 041$	null	null	null	12.07	12.03	11.64	11.06	
7	G045.4437+00.0458	$45^\circ 443, 0^\circ 045$	null	null	12.67	10.68	10.36	9.81	9.84	
8	G045.4048+00.0438	$45^\circ 404, 0^\circ 043$	null	13.65	12.17	11.04	10.99	10.58	10.6	Class III
9	G045.4274+00.0672	$45^\circ 427, 0^\circ 067$	13.11	11.64	11.07	10.53	10.49	9.94	9.63	Class III - (O-type)
10	G045.4347+00.0627	$45^\circ 434, 0^\circ 062$	null	null	null	12.77	12.54	9.40	7.81	
11	G045.3969+00.0433	$45^\circ 396, 0^\circ 043$	11.79	10.41	9.85	9.55	9.6	9.41	9.39	Class III
12	G045.4024+00.0412	$45^\circ 402, 0^\circ 041$	10.41	9.21	8.73	8.39	8.51	8.34	8.22	Class III
13	G045.3976+00.0473	$45^\circ 397, 0^\circ 047$	null	13.67	12.42	11.5	11.33	10.82	10.89	Class III
14	G045.4020+00.0361	$45^\circ 402, 0^\circ 036$	13.42	12.28	11.88	11.52	11.55	11.38	11.73	Class III - (O-type)

tron temperature in units of 10^4 K, D_{kpc} is the distance in kpc and S_ν is the flux density in Jy. Adopting an electron temperature of 10^4 K, we obtain $N_{UV} = (5 \pm 2) \times 10^{48} \text{s}^{-1}$. On the other hand, the UV photon flux corresponding to the contribution of the three stars is $\sim 3.3 \times 10^{49}$ photons per second (Martins et al. 2005). Thus, we conclude that the three stars can maintain the HII region G45L ionized and heat the dust emitting at $24 \mu\text{m}$ in the ionized gas. It is important to mention that one of the central sources by itself, #1 or #9, can provide the necessary UV photons. On the contrary, source #14 can not have created the HII region G45L alone.

Assuming that sources #1, #9, and #14 are the sources responsible for the HII region G45L, we estimate its dynamical age using a simple model described by Dyson & Williams (1980). In this model the radius of the HII region at a given time t is given by $R(t) = R_s (1 + 7 c_s t / 4 R_s)^{4/7}$, where c_s is the sound velocity in the ionized gas ($c_s = 15 \text{ km s}^{-1}$) and R_s is the radius of the Strömngren sphere, given by $R_s = (3 S_* / 4 \pi n_o^2 \alpha_B)^{1/3}$, where $\alpha_B = 2.6 \times 10^{-13} \text{ cm}^3 \text{ s}^{-1}$ is the hydrogen recombination coefficient to all levels above the ground level. S_* is the total number of ionizing photons per unit of time emitted by the stars, and n_o is the original ambient density. As a rough estimate n_o can be obtained by distributing the total molecular mass related to the structure ($M \sim 10^5 M_\odot$) over a sphere of about 7 pc ($3'$ at 8 kpc) in diameter, which yields $n_o \sim 10^4 \text{ cm}^{-3}$. Given that the actual diameter of G45L is about 7 pc, we infer that the HII region has been expanding during about $2 \times 10^6 \text{ yr}$.

3.4. Star formation around G45L

To look for primary tracers of star formation activity around G45L, we use the GLIMPSE I Spring'07 Catalog to perform photometry. Considering only sources that have been detected in the four *Spitzer*-IRAC bands, we found 151 sources in the area delimited by the dashed circle shown in Figure 10. The circular area was chosen in order to cover the molecular gas that surrounds the HII region and where the YSO candidates are expected to be located. This figure displays the spatial distribution of the YSO candidates over the *Spitzer*-IRAC $8 \mu\text{m}$ emission. The green crosses indicate Class I sources, the red boxes indicate Class II or intermediate Class I/II sources and the cyan circles indicate the sources that could be reddened Class II objects. The sources classification was performed according the photometric study presented in Figure 11, which shows the IRAC color-color diagram of the sources found. The different regions indicated correspond to different stellar evolutionary stages, as defined by Allen et al. (2004). Seventeen sources lie in the region of the protostars with circumstellar envelopes (Class I, green triangles), only 4 sources lie in the region of young stars with only disk emission (Class II and intermediate Class I/II, red triangles) and 104 sources lie in the region of the main sequence and giant stars (Class III, blue triangles). Sources represented as cyan triangles, located outside the delimited regions, could therefore be reddened Class II objects (Allen et al. 2004). Unfortunately we can not perform an additional NIR photometric study because the 2MASS data from most of these sources are either missing or given as lower limits.

In Figure 12 the same sources shown in Figure 10 are displayed over the ^{13}CO J=1-0 (left) and CS J=2-1 (right) integrated emissions between 54 and 66 km s^{-1} . Of course we do not know if all the sources seen towards G45L are at the same distance as the HII region. However, the location of some of them, mainly the Class I objects (green crosses in Figure 12), suggest that they are possibly embedded in the molecular gas related to G45L. The Class I objects lie preferently in the molecular shell and concentrate towards the East, where the CS J=2-1 emission peaks. They lie in the region where the EGO G45.47+0.05 is embedded (Cyganowski et al. 2008), confirming that in this area, southeastern the UCHII complex and eastern G45L, star formation is taking place.

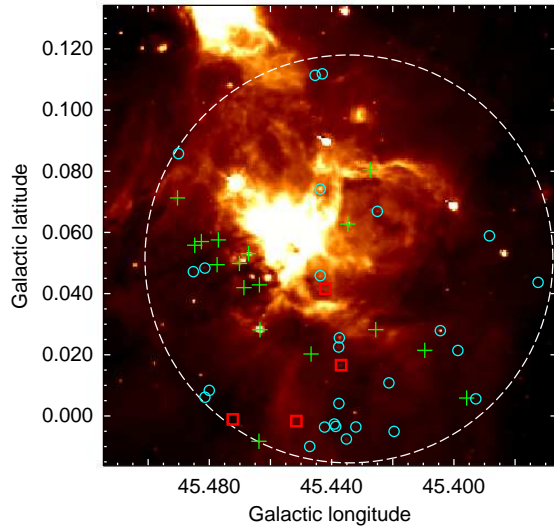


Fig. 10. *Spitzer*-IRAC $8\ \mu\text{m}$ emission with YSO candidates superimposed. Green crosses indicate Class I sources, red boxes are Class II or intermediate Class I/II sources and the cyan circles are the sources that could be reddened Class II objects. The circle encloses the region where the photometric study was performed.

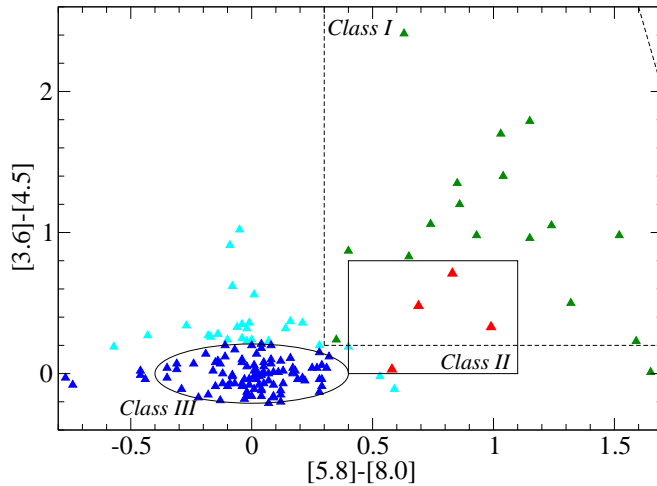


Fig. 11. GLIMPSE-IRAC color-color diagram $[3.6] - [4.5]$ versus $[5.8] - [8.0]$ for the sources observed inside the dashed circle displayed in Figure 10. As in Figure 9, Class I, II and III regions are indicated following Allen et al. (2004). In this case we consider Class I (green), Class II and intermediate Class I/II (red) and reddened Class II (cyan) objects to study star formation around G45L.

As mentioned in Section 1, Feldt et al. (1998) and Blum & McGregor (2008) identified several massive O-type stars, that are presumably on, or near, the zero-age main sequence, and are responsible for the ionization of the UCHII region G45.45+0.06. The authors also proposed that this UCHII region triggered the formation of younger UCHII regions in its surroundings, generating an UCHII complex. These studies do not mention any agent responsible for the formation of such stars. Taking into account the estimated age of G45L

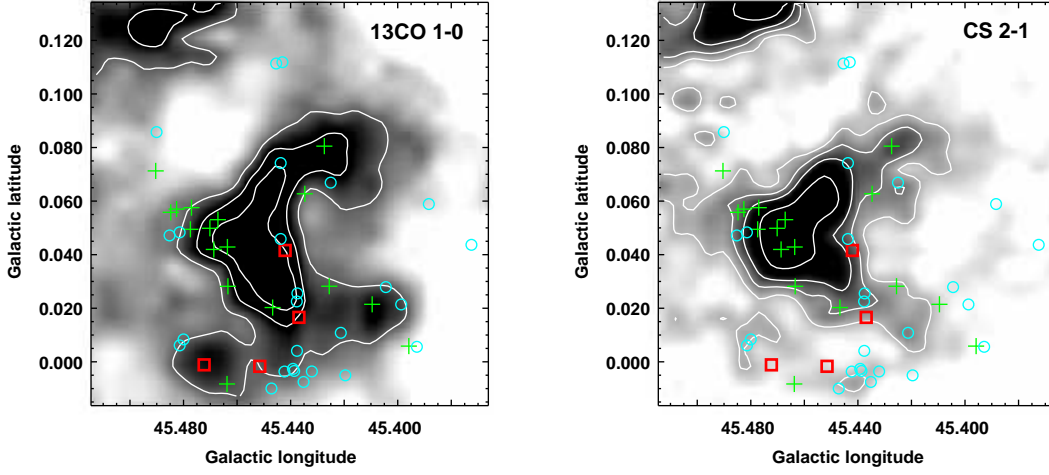


Fig. 12. Left: ^{13}CO $J=1-0$ integrated emission between 54 and 66 km s^{-1} with YSO candidates superimposed. The contour levels are 27, 37 and 48 K km s^{-1} . Right: same, but grays are the CS $J=2-1$ integrated emission in the same velocity range. The contour levels are 2.4, 3.6, 5 and 8 K km s^{-1} . Green crosses indicate Class I sources, red boxes are Class II or intermediate Class I/II sources and the cyan circles are the sources that could be reddened Class II objects.

(about 2×10^6 yr), that star formation is taking place around it, probably through the collect and collapse process, and that the UCHII complex lies on one of its border, we propose that G45L could have triggered the formation of the zero-age main sequence stars that are ionizing G45.45+0.06. However we can not discard the possibility that both HII regions, G45.45+0.06 and G45L, could be coeval.

3.5. HII region G45L spatial structure

In this section, based on the IR emission and the molecular environment study, we attempt to describe the possible spatial structure of G45L.

As described in previous sections, a view of a larger area in the vicinity of the UCHII region G45.45+0.06 reveals that it actually lies in a border of a larger and fainter HII region that we called G45L. The morphological study of G45L suggests that this HII region is far from being spherical. The observed morphology is quite complex and then projection effects should be considered to analyze the three dimensional structure. In this way, taking into account the location of the PDRs together with the spatial and velocity molecular gas distribution, we suggest that G45L has a pear-like morphology, as it is sketched in Figure 13. This figure presents two sketches of G45L possible structure as seen from two different positions. In Figure 13 (left) can be appreciated that the North PDR is composed by two structures seen superimposed along the line of sight and the middle PDR is the projection of the southern border of the HII region portion closer to us. The UCHII complex that lies towards the East of G45L is represented as a red cloud. Figure 13 (right) shows a longitudinal cut of G45L remarking the molecular gas components related to the PDRs. As the molecular analysis shows, the structure delimited by the North and the middle PDRs has associated molecular gas centered at $v \sim 55 \text{ km s}^{-1}$, while the structure delimited by the South and the North PDRs has associated molecular gas centered at $v \sim 59 \text{ km s}^{-1}$.

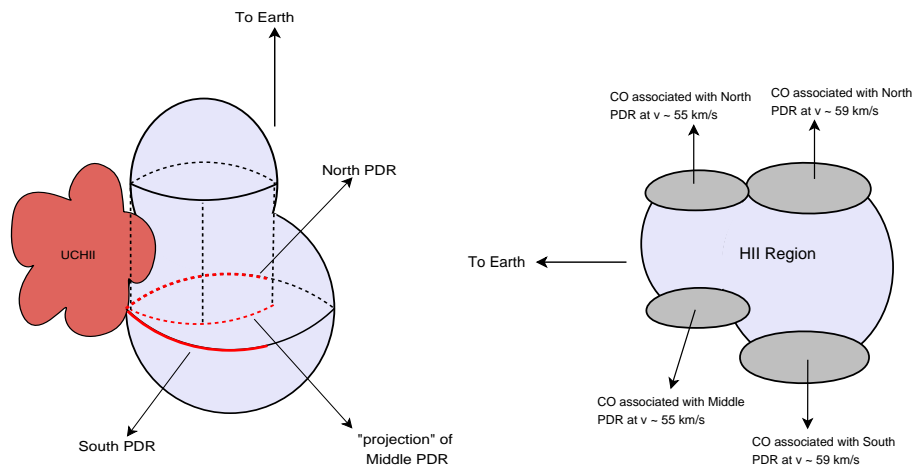


Fig. 13. Left: sketch of the possible shape of the HII region G45L. The PDRs are remarked. The UCHII complex is represented as a red cloud. Right: a longitudinal cut of G45L remarking the molecular gas components related to the PDRs.

Most ionized nebulae, in particular HII regions, have complex morphologies structures (Morisset et al. 2005). There are many physical causes that may account for such morphologies. Some causes for the G45L spatial structure could be: the presence of density gradients in the ISM where the HII region is evolving, the existence of more than one exciting star, the fact that these exciting stars could have high spatial velocities with respect to the local ISM, and the effects of possible stellar and/or interstellar magnetic fields.

4. Summary

Using multiwavelength survey and archival data, we studied the ISM towards a region about $7' \times 7'$ in the vicinity of the G45.45+0.06 UCHII complex. The main results can be summarized as follows:

(a) We found that the UCHII complex lies in a border of a larger ($\sim 3'$ of diameter) and fainter HII region, here named G45L.

(b) Although G45L is not completely border by a PDR, its morphology resembles the structure of the IR dust bubbles associated with O and early-B type stars: a PDR visible in the $8 \mu\text{m}$ band, which encloses ionized gas observed at 20 cm and hot dust observed at $24 \mu\text{m}$.

(c) We find a good morphological correlation between the PDRs and the molecular gas, which suggests that the HII region may be collecting the molecular material.

(d) Taking into account the velocity ($v_{\text{LSR}} \sim 55 - 60 \text{ km s}^{-1}$) of the molecular gas related to G45L and the HI absorption study, we conclude that this HII region is at the same distance as the UCHII complex, $\sim 8 \text{ kpc}$.

(e) The PDRs position and the spatial and velocity distribution of the associated molecular shell suggest that G45L has a pear-like morphology.

(f) From a near- and mid-IR photometric study, we found three sources, likely O-type stars (between O4V and O8V) that are possibly responsible for the creation of G45L.

Additionally we found several YSO candidates lying preferentially in the molecular shell and concentrating towards the East where the CS J=2–1 emission peaks. Our results confirm that the southeastern region of the UCHII complex where G45.45+0.06 is embedded (eastern part of G45L) is an active star formation region.

(g) Assuming that three O-type stars are responsible of G45L, we suggest this HII region has been expanding during about 2×10^6 yr and could have triggered the formation of the zero-age main sequence stars that are ionizing the UCHII region G45.45+0.06. However we can not discard that both HII regions are coeval.

Acknowledgements. We wish to thank the anonymous referee whose comments and suggestions have helped to improve the paper. S.P. and S.C. are members of the *Carrera del investigador científico* of CONICET, Argentina. M.O. is a doctoral fellow of CONICET, Argentina. This work was partially supported by the CONICET grant PIP 112-200801-02166, UBACYT A023 and ANPCYT PICT-2007-00902 and -00812.

References

- Allen, L. E., Calvet, N., D’Alessio, P., et al. 2004, *ApJS*, 154, 363
- Anderson, L. D., Bania, T. M., Jackson, J. M., et al. 2009, *ApJS*, 181, 255
- Blum, R. D. & McGregor, P. J. 2008, *AJ*, 135, 1708
- Chaisson, E. J. 1976, in *Frontiers of Astrophysics*, 259–351
- Churchwell, E., Povich, M. S., Allen, D., et al. 2006, *ApJ*, 649, 759
- Churchwell, E., Watson, D. F., Povich, M. S., et al. 2007, *ApJ*, 670, 428
- Cichowski, S., Romero, G. A., Ortega, M. E., Cappa, C. E., & Vasquez, J. 2009, *MNRAS*, 394, 900
- Codella, C., Lorenzani, A., Gallego, A. T., Cesaroni, R., & Moscadelli, L. 2004, *A&A*, 417, 615
- Cutri, R. M., et., & al., 2003, 2MASS All Sky Catalog of point sources (The IRSA 2MASS All-Sky Point Source Catalog, NASA/IPAC Infrared Science Archive. <http://irsa.ipac.caltech.edu/applications/Gator/>)
- Cyganowski, C. J., Whitney, B. A., Holden, E., et al. 2008, *AJ*, 136, 2391
- Deharveng, L., Lefloch, B., Kurtz, S., et al. 2008, *A&A*, 482, 585
- Deharveng, L., Zavagno, A., & Caplan, J. 2005, *A&A*, 433, 565
- Dyson, J. E. & Williams, D. A. 1980, *Physics of the interstellar medium* (New York, Halsted Press, p. 204)
- Fazio, G. G., Hora, J. L., Allen, L. E., et al. 2004, *ApJS*, 154, 10
- Feldt, M., Stecklum, B., Henning, T., et al. 1998, *A&A*, 339, 759
- Garay, G., Rodriguez, L. F., Moran, J. M., & Churchwell, E. 1993, *ApJ*, 418, 368
- Giveon, U., Becker, R. H., Helfand, D. J., & White, R. L. 2005a, *AJ*, 129, 348
- Giveon, U., Becker, R. H., Helfand, D. J., & White, R. L. 2005b, *AJ*, 130, 156
- Goicoechea, J. R., Pety, J., Gerin, M., et al. 2006, *A&A*, 456, 565
- Hatchell, J., Thompson, M. A., Millar, T. J., & MacDonald, G. H. 1998, *A&AS*, 133, 29
- Jackson, J. M., Rathborne, J. M., Shah, R. Y., et al. 2006, *ApJS*, 163, 145
- Johnstone, D., Boonman, A. M. S., & van Dishoeck, E. F. 2003, *A&A*, 412, 157
- Kolpak, M. A., Jackson, J. M., Bania, T. M., Clemens, D. P., & Dickey, J. M. 2003, *ApJ*, 582, 756
- Luna, A., Bronfman, L., Carrasco, L., & May, J. 2006, *ApJ*, 641, 938
- Martins, F. & Plez, B. 2006, *A&A*, 457, 637
- Martins, F., Schaerer, D., & Hillier, D. J. 2005, *A&A*, 436, 1049
- Matthews, H. E., Goss, W. M., Winnberg, A., & Habing, H. J. 1977, *A&A*, 61, 261
- Morisset, C., Stasińska, G., & Peña, M. 2005, *MNRAS*, 360, 499
- Ohashi, N., Kawabe, R., Ishiguro, M., & Hayashi, M. 1991, *AJ*, 102, 2054
- Pomarès, M., Zavagno, A., Deharveng, L., et al. 2009, *A&A*, 494, 987
- Remijan, A., Shiao, Y.-S., Friedel, D. N., Meier, D. S., & Snyder, L. E. 2004, *ApJ*, 617, 384
- Simon, R., Jackson, J. M., Clemens, D. P., Bania, T. M., & Heyer, M. H. 2001, *ApJ*, 551, 747
- Stil, J. M., Taylor, A. R., Dickey, J. M., et al. 2006, *AJ*, 132, 1158

- Watson, C., Povich, M. S., Churchwell, E. B., et al. 2008, *ApJ*, 681, 1341
- Werner, M. W., Roellig, T. L., Low, F. J., et al. 2004, *ApJS*, 154, 1
- White, R. L., Becker, R. H., & Helfand, D. J. 2005, *AJ*, 130, 586
- Wilner, D. J., Ho, P. T. P., & Zhang, Q. 1996, *ApJ*, 462, 339
- Wood, D. O. S., Churchwell, E., & Salter, C. J. 1988, *ApJ*, 325, 694
- Zavagno, A., Pomarès, M., Deharveng, L., et al. 2007, *A&A*, 472, 835